

Measurement-Induced Phase Transition in State Estimation of Chaotic Systems and the Directed Polymer

Federico Gerbino,¹ Guido Giachetti,² Pierre Le Doussal,² and Andrea De Luca³

¹*Laboratoire de Physique Théorique et Modèles Statistiques,
Université Paris-Saclay, CNRS, 91405 Orsay, France*

²*Laboratoire de Physique de l'École Normale Supérieure, CNRS, ENS & PSL University,
Sorbonne Université, Université Paris Cité, 75005 Paris, France*

³*Laboratoire de Physique Théorique et Modélisation, CY Cergy Paris Université,
CNRS, 95302 Cergy-Pontoise, France*

We introduce a solvable model of a measurement-induced phase transition (MIPT) in a deterministic but chaotic dynamical system with a positive Lyapunov exponent. In this setup, an observer only has a probabilistic description of the system but mitigates chaos-induced uncertainty through repeated measurements. Using a minimal representation via a branching tree, we map this problem to the directed polymer (DP) model on the Cayley tree, although in a regime dominated by rare events. By studying the Shannon entropy of the probability distribution estimated by the observer, we demonstrate a phase transition distinguishing a chaotic phase with reduced Lyapunov exponent from a strong-measurement phase where uncertainty remains bounded. Remarkably, the location of the MIPT transition coincides with the freezing transition of the DP, although the critical properties differ. We provide an exact universal scaling function describing entropy growth in the critical regime. Numerical simulations confirm our theoretical predictions, highlighting a simple yet powerful framework to explore measurement-induced transitions in classical chaotic systems.

Introduction. — In recent years, much attention has been devoted to the complex effects generated by the combination of unitary evolution with external noise [1–9], particularly considering that induced by the action of quantum, projective, or weak measurements [10]. It is well established that in its evolution a closed quantum system tends to encode local information into nonlocal degrees of freedom, resulting in the production of entanglement entropy and eventually thermalization [11–15]; in contrast, measurements of local quantities compete by extracting information from the quantum state. From this interplay, as the effectiveness and frequency of the measurements vary, two phases can emerge [16–18]: at weak measurements, the system remains resilient to the action of the measurements [19, 20], thus exhibiting a spontaneous error-correcting capacity [21–23] and visiting quantum states that are difficult to simulate classically (volume law); at strong measurements, on the other hand, information remains confined to local degrees of freedom, entanglement cannot grow beyond a threshold (area law), and an effective description in terms of matrix product states is possible [24]. From a statistical physics point of view, this transition falls into the realm of disordered systems because of the inherently random outcome of quantum measures, with one important difference: the distribution of outcomes is not fixed a priori but is determined by the state itself (according to Born's rule). This results in a difference in the $n \rightarrow 1$ replica limit [25] from the usual $n \rightarrow 0$ of ordinary disordered systems [26, 27]. For non-interacting fermions [28–35], this formulation has revealed similarities with the Anderson transition [36] and an effective description in terms of a non-linear sigma model [37, 38]. Not surprisingly,

an accurate characterization of the critical point for the interacting case is difficult, although approaches, more or less controlled, based on annealed averages [39–44], mean field [45–47], random matrices [48, 49], field theory [50–52] and numerics [53–56], have yielded various insights. Beyond the theoretical and computational relevance, experiments have confirmed this phenomenology [57–59], although the observability of this transition in extended systems has been a cause for discussion because of the burden of post-selection [60, 61].

A similar protocol can also be considered in a purely classical context, where a stochastic evolution is updated by measurements according to Bayes' theorem [62, 63]; for a 1D diffusive particle undergoing Bayesian monitoring, a short-time KPZ behavior has been suggested while the long-time behavior remained elusive [64]. In this Letter, we present a simple, solvable model exhibiting a phase transition. To formulate it, it is useful to think of a generic deterministic but chaotic dynamical system, thus characterized by a positive Lyapunov exponent that controls the growth of uncertainty about the actual state of the system. Thus, although the state of the system is deterministic, chaos in the presence of finite precision allows only a probabilistic description. However, to mitigate this uncertainty, an observer makes measurements of the system state that they use to update their estimate of the system state. We consider a minimal description of this setup through a branching tree, in which the branching ratio K is related to the (maximum) Lyapunov exponent, see Fig. 1. This formulation allows a mapping to the famous directed polymer problem in this geometry [65]. However, the aforementioned $n \rightarrow 1$ limit, associated with the correct probability of measurements

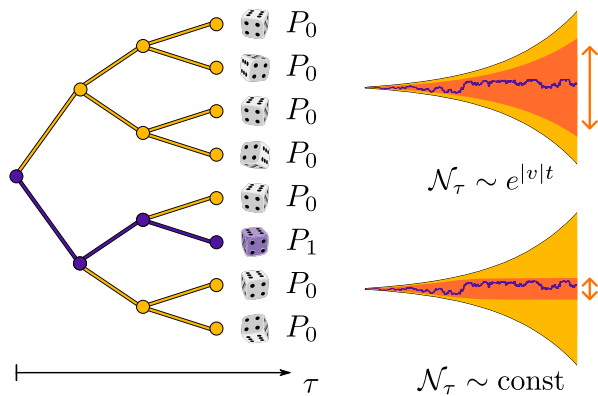


FIG. 1. *Left:* Cayley tree ($K = 2$), modeling the exponential growth $\Delta x_{\max} \sim e^{\lambda t}$ of the uncertainty in the position of a particle. The purple branch depicts the true trajectory x_τ of the particle: at each time-step τ , a finite-precision measurement on each site is performed, whose outcomes a_j are distributed with $P_{n_j}(a_j)$ depending on the occupancy of the site j , $n_j = 0, 1$. *Right:* sketch of the two phases of the model. The dark-yellow region represents a subregion of size $\mathcal{N}_\tau \sim e^{S t}$ in which the observer can be reasonably sure the particle is located. The effectiveness of measurements, as quantified by the Kullback-Leibler divergence between $P_0(a)$ and $P_1(a)$, determines whether $\mathcal{N}_\tau \sim \text{const}$ or \mathcal{N}_τ still scale exponentially, but with a reduced Lyapunov exponent $|v| < \lambda$.

outcomes, requires to analyze this problem in a regime of rare events [66]. We avoid the technical difficulties of the replica limit [67], through the study of the Shannon entropy of the observer-estimated probability distribution: we demonstrate the existence of a phase transition, reminiscent of the quantum one between (i) a regime in which the chaos persists albeit with a reduction in the effective Lyapunov exponent, and (ii) a regime in which the uncertainty saturates with time. Quite interestingly, the location of the transition separating these two phases coincides with one of the freezing transition of the DP. In addition, we are able to thoroughly characterize the critical regime by providing an explicit, exact and universal scaling function that describes the entropy growth at long times. We note that, in contrast with quantum MIPT, there is no post-selection barrier since the measurements do not affect the actual state of the system. Indeed, our numerical simulations fully confirm the predictions.

The model — We begin by abstractly formulating an observer describing a dynamical system. The possible states of the system are associated to the nodes of a graph, so that the evolution of the configuration of the system is seen as a particle hopping along the edges. To model the spreading of uncertainty in our chaotic setting, we assume the graph is a Cayley tree with branching factor K along the effective discrete-time direction $t = \tau \Delta t$. As the evolution is deterministic, the configuration of the system follows a specific path connecting the root to a leaf. However, an external observer with finite precision

has no access to the specific path and can only rely on a probabilistic description: we denote as $p_j^{(\tau)}$ the probability that the particle is located in j at time-step τ . We assume for simplicity that a-priori every branching is equiprobable, so that the particle undergoes a “directed” random walk. Specifically, assuming the particle lies in $x_\tau \in \{j\}_{j=1}^{K^\tau}$ at time-step τ , during $t \rightarrow t + \Delta t$, it hops to one of the K possible states $K(x_\tau - 1) + m$ at level $\tau + 1$, with $m \in \{1, \dots, K\}$. Let us notice that, by setting $K = e^{\lambda \Delta t}$, the maximum separation between two trajectories at time t is $\Delta x_{\max} \sim e^{\lambda t}$ so that λ can be identified with the maximal Lyapunov exponent. Right after the random walk step, the observer performs instantaneous measurements of each site in order to mitigate the growth of uncertainty. In order to measure site j at time-step τ , a measuring apparatus returns a value $a_j^{(\tau)}$ correlated with the presence or absence of the particle at that site. In practice, $a_j^{(\tau)}$ is a random variable whose probability distribution is $P_1(a)$ if the site is indeed occupied at time-step τ and $P_0(a)$ otherwise. While the outcome of each measurement is not deterministic, the measurement is classical, so that the system is unaffected by it. Accordingly, measurements from different sites are statistically independent, and we obtain the probability of outcomes $\mathbf{a}^{(\tau)} \equiv \{a_j^{(\tau)}\}_{j=1}^{K^\tau}$ conditioned to the particle being in site j as

$$P(\mathbf{a}^{(\tau)} | x_\tau = j) = \frac{P_1(a_j^{(\tau)})}{P_0(a_j^{(\tau)})} \prod_{j'=1}^{K^\tau} P_0(a_{j'}^{(\tau)}). \quad (1)$$

From the knowledge of the measurement outcomes $\mathbf{a}^{(\tau+1)}$ at level $\tau + 1$, the observer can update the estimate of the probabilities from p_j^τ to $p_j^{(\tau+1)}$ using Bayes’ theorem

$$p_j^{(\tau+1)} = \frac{P(\mathbf{a}^{(\tau+1)} | j) p_j^{(\tau+1,-)}}{\sum_{j'} P(\mathbf{a}^{(\tau+1)} | j') p_{j'}^{(\tau+1,-)}}, \quad p_j^{(\tau+1,-)} = \frac{p_{\lceil j/K \rceil}^{(\tau)}}{K} \quad (2)$$

where $p_j^{(\tau+1,-)}$ indicates the probabilities right before the measurements, $p_j^{(\tau+1)}$ are the probabilities after the measurements, and $\lceil \dots \rceil$ denotes the ceiling function. The second equation in (2) accounts for the equiprobable hopping of the particle from level τ to $\tau + 1$. According to Eq. (1), the distribution of outputs $\mathbf{a}^{(\tau+1)}$ in (2) depends on the true trajectory of the particle. In the spirit of repeating the whole experiment many times, a finite precision in fixing the initial condition results in an ensemble of true trajectories, which we take uniform distributed among all those on the tree. Thus, the probabilities $p_j^{(\tau+1)}$ are now in turn random variables, depending on the specific realization of the $a_j^{(\tau')}$ with $\tau' \leq \tau + 1$: our focus is their statistical properties. For this purpose [68], the trajectory x_τ can be generated on the fly by sampling the ending point from the $p_j^{(\tau)}$ themselves. This implies

that the $a_j^{(\tau+1)}$ in (2) are drawn at step $\tau + 1$ with a probability distribution which only depends on the probabilities $\mathbf{p}^{(\tau+1,-)} \equiv \{p_j^{(\tau+1,-)}\}_{j=1}^{K^{\tau+1}}$ and which reads

$$P(\mathbf{a}^{(\tau+1)} | \mathbf{p}^{(\tau+1,-)}) = \sum_j P(\mathbf{a}^{(\tau+1)} | j) p_j^{(\tau+1,-)}. \quad (3)$$

Eqs. (2, 3) then fully determine the joint stochastic evolution of the probabilities $\mathbf{p}^{(\tau)} \rightarrow \mathbf{p}^{(\tau+1)}$.

Mapping to a directed polymer — Due to the denominator, Eq. (2) is patently nonlinear, and couples p_j at different sites. To get rid of these difficulties, we work with non-normalized random variables $\mathbf{z}^{(\tau)} \equiv \{z_j^{(\tau)}\}_{j=1}^{K^\tau}$ chosen to evolve as $z_j^{(\tau+1,-)} = z_{\lfloor j/K \rfloor}^{(\tau)} / K$, and $z_j^{(\tau+1)} = P_1(a_j^{(\tau+1)}) / P_0(a_j^{(\tau+1)}) z_j^{(\tau+1,-)}$. Setting initially $z_0^{(\tau=0)} = p_0^{(\tau=0)}$, the original probabilities can be recovered via normalization $p_j^{(\tau)} = z_j^{(\tau)} / Z^{(\tau)}$, where $Z^{(\tau)} = \sum_{j=1}^{K^\tau} z_j^{(\tau)}$. Additionally, one can show [68] that expectation values (denoted by brackets) of a generic function $F[\{p\}]$ of the $p_j^{(\tau)}$'s evolved with Eqs. (2,3) can be expressed as

$$\langle F[\{p_j^{(\tau)}\}] \rangle = \left\langle F \left[\left\{ \frac{z_j^{(\tau)}}{Z^{(\tau)}} \right\} \right] Z^{(\tau)} \right\rangle_0, \quad (4)$$

where $\langle \dots \rangle_0$ denotes the process where all $a_j^{(\tau)}$ are i.i.d. with distribution $P_0(a)$. $Z^{(\tau)}$ can also be interpreted as a weight which modifies the probability of each realization of the outcomes \mathbf{a} and consistently the normalization of the $p_j^{(\tau)}$'s implies $\langle Z^{(\tau)} \rangle_0 = 1 \forall \tau \geq 0$.

In this formalism, we can associate to each node in the tree a random Boltzmann weight $B(a) := P_1(a) / (K P_0(a))$ with a drawn from $P_0(a)$, so that $z_j^{(\tau)}$ equals the product of Boltzmann weights along the path from root to the leaf j at level τ . It is common to interpret these paths as configurations of a directed polymer on the tree, so that $Z^{(\tau)}$ is the corresponding partition function [69].

Entropy dynamics — Our goal is now to determine whether the observer is able to effectively locate the particle. Intuitively, it is clear that the more the two $P_{0,1}(a)$ distributions differ, the more the observer will be able to discern where the particle is, typically resulting in a set of $p_j^{(\tau)}$ peaked around few j 's. A quantifier of the effectiveness of the measurement protocol is the so-called Kullback-Leibler divergence of $P_1(a)$ with respect to $P_0(a)$, $D_{\text{KL}}(P_1 \| P_0) := \langle \ln(P_1(a)/P_0(a)) \rangle_1 > 0$, where $\langle \dots \rangle_1 = \int da \dots P_1(a)$, which precisely measures the surprise of an observer to find that a is distributed according to $P_1(a)$, while $P_0(a)$ is expected. We will see how D_{KL} acts as a knob for the MIPT in this protocol. To this aim, we evaluate the growth in time of the average Shannon entropy $\langle S_t \rangle = \left\langle - \sum_{j=1}^{K^\tau} p_j^{(\tau)} \ln p_j^{(\tau)} \right\rangle$ which quantifies the degree of uncertainty on the particle location. More specifically, one can think of $\mathcal{N}_\tau \sim e^{S_t}$ as an

estimate of the number of sites in which the probability of finding the particle is significantly different from zero. According to Eq. (4) it can be expressed as

$$\langle S_t \rangle = \left\langle Z^{(\tau)} \ln Z^{(\tau)} \right\rangle_0 - \sum_{j=1}^{K^\tau} \left\langle z_j^{(\tau)} \ln z_j^{(\tau)} \right\rangle_0. \quad (5)$$

The second term in this expression can be promptly computed as each $z_j^{(\tau)}$ is expressed as the product of independent factors leading to $\sum_{j=1}^{K^\tau} \left\langle z_j^{(\tau)} \ln z_j^{(\tau)} \right\rangle_0 = vt$ where we introduced (see End Matter (EM))

$$v := \frac{1}{\Delta t} D_{\text{KL}}(P_1 \| P_0) - \lambda, \quad (6)$$

which can be seen as a control parameter accounting for the competition between the measurement precision and the chaotic spread of the trajectories quantified by the Lyapunov exponent $\lambda = \ln K / \Delta t$.

In contrast, the first term in the r.h.s. of Eq. (5) is more involved. We first observe that it differs from the usual calculation of the free energy $\propto \ln Z$ in quenched-disorder problems, as a consequence of Bayes' theorem (2) and (4). In contrast, in Eq. (5), one can express $Z \ln Z = \partial_n Z^n |_{n=1}$ so that the entropy is written as the difference between the $n \rightarrow 1$ replicated polymer partition function with ‘‘point-to-line’’ and with ‘‘point-to-point’’ boundary conditions. Here, instead we avoid replicas and consider the distribution of the directed polymer partition function $Z^{(\tau)}$. In general, this is a difficult problem since the configurations entering $Z^{(\tau)}$ have different degrees of correlation based on how much the different paths overlap. For the tree, this difficulty can be solved using self-similarity as in Ref. [65]: we observe that a tree of level $\tau + 1$ can be obtained by juxtaposing K independent trees of level τ and connecting their vertices with a branching point. In terms of the $Z^{(\tau)}$, this leads to the recurrence relation

$$Z^{(\tau+1)} \stackrel{\text{in law}}{=} B(a) \sum_{\kappa=1}^K Z_\kappa^{(\tau)}, \quad (7)$$

where the $Z_\kappa^{(\tau)}$'s are K independent realizations of $Z^{(\tau)}$, a is drawn from $P_0(a)$ and the equality is meant in law for probability distributions. Eq. (7) can be turned into a deterministic recursive equation for the Laplace transform $G_\tau(y) := \langle \exp(-e^{-y} Z^{(\tau)}) \rangle_0$

$$G_{\tau+1}(y) = \left\langle G_\tau(y - \ln B(a))^K \right\rangle_0. \quad (8)$$

The evolution equation (8) belongs to a wide class of nonlinear reaction-diffusion equations including the famous Kolmogorov-Petrovsky-Piskunov (KPP) equation valid for continuous space and time (see below). Quite generally, the solution $G_\tau(y)$ behaves as a ballistically moving stationary wavefront, monotonically interpolating between $G_\tau(-\infty) = 0$ and $G_\tau(\infty) = 1$. This traveling stationary solution characterises the distribution of $\ln Z^{(\tau)}$

for large τ around its typical value. In our case however, it is more convenient to rewrite $G_\tau(y) = 1 - e^{-y}u_\tau(y)$. Because of the normalization condition $\langle Z^{(\tau)} \rangle_0 = 1$, $G_\tau(y) = 1 - e^{-y} + O(e^{-2y})$ and $u_\tau(+\infty) = 1$, while from $G_\tau(y \rightarrow -\infty) \rightarrow 0$, we deduce $u_\tau(y \rightarrow -\infty) \sim e^y \rightarrow 0$. In terms of this function, we express (see EM)

$$\langle Z^{(\tau)} \ln Z^{(\tau)} \rangle_0 = \int_{-\infty}^{\infty} dy (u_0(y) - u_\tau(y)). \quad (9)$$

Entropy growth rate — While our model is formulated for $K = e^{\lambda\Delta t} \in \mathbb{N}$, Eq. (8) allows us to take the continuous time limit $\Delta t \rightarrow 0$ while $\lambda = O(1)$. Consistently, as suggested by the control parameter v defined by Eq. (6), the accuracy of the measurements has to be scaled choosing $P_1(a) = P_0(a) + O(\sqrt{\Delta t})$. As shown in the EM, this corresponds to setting $D_{\text{KL}}(P_1 \parallel P_0) = \sigma^2\Delta t/2$, which is the only residual parameter of the finer structure of $P_1(a)$, $P_0(a)$. This limit is useful to simplify the discussion from a technical point of view, although it is not strictly necessary as the same phenomenology can be obtained while keeping time discrete (see EM). Setting $G_\tau(y) = 1 - h_t(y)$, in the $\Delta t \rightarrow 0$ limit, Eq. (8) assumes the more familiar form of the KPP equation

$$\partial_t h = \frac{\sigma^2}{2} \partial_y^2 h + (\lambda + \sigma^2/2) \partial_y h + \lambda F(h) \quad (10)$$

where $F(h) = -(1-h)\ln(1-h)$. Beyond this specific form, the results will be universal, given some general properties such as that $F(0) = F(1) = 0$, with $F'(0) = 1$ and $F''(h) < 0$, implying that $h = 1$ and $h = 0$ are fixed points, respectively stable/unstable. At long times there are two cases: For $\sigma \geq \sqrt{2\lambda}$ the solution behaves as a traveling wave, $h_t(y) \simeq \bar{h}(y - y_t)$ with $y_t \simeq v_{\text{KPP}}t - \frac{2\alpha\sigma}{\sqrt{2\lambda}} \ln t + o(1)$ and the translation speed $v_{\text{KPP}} = -(\frac{\sigma}{\sqrt{2}} - \sqrt{\lambda})^2$; for $\sigma < \sqrt{2\lambda}$, it converges to a limit $h_t(y) \rightarrow h_\infty(y)$ and $v_{\text{KPP}} = 0$ [70]. However, it is more relevant for us to take the $\Delta t \rightarrow 0$ of Eq. (9) setting $u_t(y) := e^y h_t(y) = u_\tau(y)$ and considering the corresponding partial differential equation

$$\partial_t u_t(y) = -v \partial_y u_t(y) + \frac{\sigma^2}{2} \partial_y^2 u_t(y) - \lambda e^y \tilde{F}(e^{-y}u), \quad (11)$$

where $\tilde{F}(h) := h - F(h)$ and $v = \sigma^2/2 - \lambda$ comes from the continuum limit of Eq. (6). In the limit of non-informative measurements $\sigma \rightarrow 0$, the entropy grows linearly as $\langle S_t \rangle = \lambda t$. So, we first discuss the asymptotic rate of entropy production $s := \lim_{t \rightarrow \infty} \langle S_t \rangle / t$. In this perspective, since $u_t(y) e^{-y} \xrightarrow{y \rightarrow -\infty} 1$, for any fixed y_0 , the contribution of the $y < y_0$ to the integral in the r.h.s. of Eq. (9) is $O(1)$ in time. It is thus inessential to the calculation of the rate which is instead controlled by large positive y . In this regime, $h(y) \ll 1$ and since $\tilde{F}(h) = O(h^2)$ at small h , we can neglect the non-linear part in Eq. (11). As u_t grows from 0 to 1, we can interpret $u_t(y)$ as the cumulative probability distribution of a

Wiener process with drift v and diffusion constant $\sigma^2/2$. Thus, in this linearized approximation, $u_t(y)$ translates at velocity v while broadening diffusively. For $v \neq 0$, the drift is the dominant factor (see inset in Fig. 2): for $v > 0$, the integral in Eq. (9) $\sim vt$; conversely, for $v < 0$ the wavefront exits the domain of integration $y > 0$, and in Eq. (5) $\langle Z^{(\tau)} \ln Z^{(\tau)} \rangle_0 \rightarrow O(1)$, (the precise value can be computed in an expansion at small σ^2 , see [68]). From these considerations, we deduce the exact growth rate

$$s := \lim_{t \rightarrow \infty} \frac{\langle S_t \rangle}{t} = \begin{cases} |v| & v \leq 0 \\ 0 & v > 0 \end{cases}. \quad (12)$$

As anticipated, the velocity v tunes a continuous phase transition of the rate of entropy production. Note that the diffusive front described by Eq. (11) should not be confused with the traveling wave $h_t(y) = \bar{h}(y - y_t)$ from (10): in $h_t(y)$, the front $u_t(y)$ is visible only as an exponentially suppressed far tail at very large y [68]. In particular, for $\sigma \geq \sqrt{2\lambda}$, $v_{\text{KPP}} < 0$ and $v > 0$ so that the two fronts move in opposite directions, a manifestation of the fact that $\langle Z^{(\tau)} \ln Z^{(\tau)} \rangle_0$ is controlled by rare instances of $\ln Z^{(\tau)}$. Instead, when $\sigma < \sqrt{2\lambda}$, $v_{\text{KPP}} = 0$ and $v < 0$: this indicates that the propagation to the left of $u_t(y) = e^y h_t(y)$ must eventually stop due to nonlinearity (see Fig. 2 inset), although this has no effect on the growth rate s . At $v = 0$, the front (11) broadens diffusively, so one expects $\langle S_t \rangle = O(\sqrt{t})$. However, in that critical case, a more careful analysis of the nonlinearity is needed as we explain below.

Critical regime — For small $v < 0$, equating $|v|t_v \sim \sqrt{t_v}$, one needs $t \gtrsim t_v = |v|^{-2}$, to distinguish the critical behavior from the linear growth. This suggests to consider the limit $v \rightarrow 0$, $t \rightarrow \infty$ while keeping the rescaled time $T = v^2 t / \sigma^2$ fixed. From the diffusive part in Eq. (11), one sees that we also have to scale the space variable as $Y = y|v|/\sigma^2$ and consider $U_T(Y) = u_t(y)$. Let us analyze the effect of the nonlinearity in this limit: for $Y > 0$, it becomes negligible as $e^{\sigma^2 Y / |v|} \tilde{F}(e^{-\sigma^2 Y / |v|} u) \sim e^{-\sigma^2 Y / |v|} u^2 \rightarrow 0$; on the other hand for $Y < 0$, as $0 < h_\tau(y) < 1$, $U_T(Y) < e^{-\sigma^2 |Y| / |v|} \xrightarrow{v \rightarrow 0} 0$. In other words, $U_T(Y)$ satisfies drifted diffusion for $Y > 0$ but with a wall imposing $U_T(Y \leq 0) = 0$. Since furthermore $U_T(+\infty) = 1$, one can interpret $U_T(Y)$ as the cumulative probability of a drifted Wiener process with a reflecting wall at $Y = 0$. Its expression can be computed explicitly (see EM), leading to the following asymptotic large time behavior close to criticality

$$\langle S_t \rangle \simeq \frac{\sigma^2}{v} \mathcal{S} \left(v \sqrt{\frac{t}{2\sigma^2}} \right) \quad (13)$$

with the scaling function

$$\mathcal{S}(\eta) = \left(\frac{1}{2} + \eta^2 \right) \operatorname{erf} \eta - \eta^2 + \frac{\eta}{\sqrt{\pi}} e^{-\eta^2}. \quad (14)$$

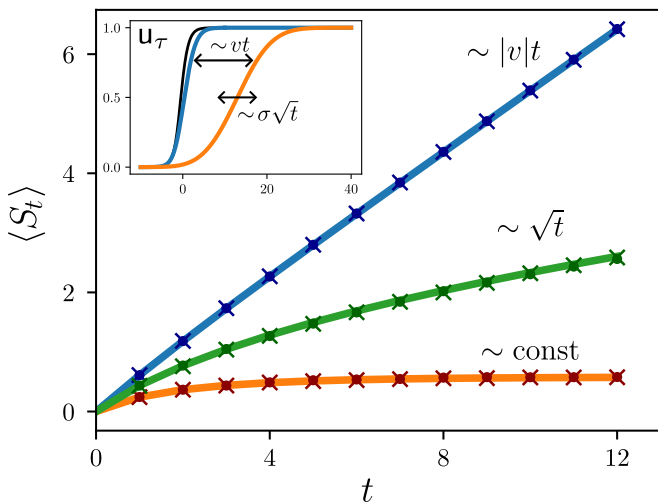


FIG. 2. Numerical analysis with $K = 2$ and $P_0(a) \sim \mathcal{N}(0, 1)$ a zero-centered Gaussian, with $P_1(a) \sim \mathcal{N}(\epsilon, 1)$, so that $D(P_1||P_0) = \text{Var}(P_1||P_0)/2 = \epsilon^2/2$ [68]. For $v < 0$, the average entropy $\langle S_t \rangle \sim |v|t$ grows linearly in time (blue, $v = -0.51$); for $v > 0$, $\langle S_t \rangle$ reaches a constant finite value (orange, $v = 0.93$). For $v = 0$, $\langle S_t \rangle \propto \sqrt{t}$ (green). Dots and crosses display the average entropy $\langle S_t \rangle$ from trajectories of the physical particle x_τ and of the evolved probabilities (2), respectively [68]. Thick continuous lines show the entropy (5) obtained numerically solving Eqs. (8) and (9) for $u_\tau(y) = e^y(1 - G_\tau(y))$. Inset: the solution of Eq. (11) is compared to the initial condition (black). For $v > 0$ (orange), the drift and broadening is clearly visible. For $v < 0$, the solution converges to a limiting form $u_t(y) \rightarrow e^y h_\infty(y)$.

For $v = 0$ this gives $\langle S_t \rangle = \sigma\sqrt{2t/\pi}$, while in the regimes $\eta \rightarrow \pm\infty$, we recover Eq. (12) for $v > 0$ and $v < 0$ respectively. Moreover, we can now compute the critical scaling of $\langle S_t \rangle$, namely $\langle S_t \rangle \sim \sigma^2/(2v)$ for $v \rightarrow 0^+$ and $\langle S_t \rangle \sim |v|t + \sigma^2/(2|v|)$ for $v \rightarrow 0^-$ consistently with Eq. (12). Note that Eq. (13) and the scaling form (14) are completely universal in our protocol and also apply to the discrete case where v is given by Eq. (6), while $\sigma^2 = \text{Var}(P_1||P_0)/\Delta t$ with $\text{Var}(P_1||P_0) := \langle \ln^2(P_1(a)/P_0(a)) \rangle_1 - \langle \ln(P_1(a)/P_0(a)) \rangle_1^2$. Indeed, a comparison with the numerics performed on the discrete model shows perfect agreement (see Fig. 3).

Conclusions — In this Letter, we considered the competition between exponential spreading of uncertainty and Bayesian updating of information by repeated measures. We introduced a toy model in terms of the directed random walk of a particle on a tree and obtain a connection to the DP on the Cayley tree. We can then employ the many tools available for this framework, but with significant differences due to the reweighting of polymer configurations due to Bayes' theorem. Our results can be regarded both as a simple and solvable example of a MIPT for a classical particle on the tree and as a fascinating transition in chaos mitigation. Interestingly, we find that the critical point for the MIPT discussed here

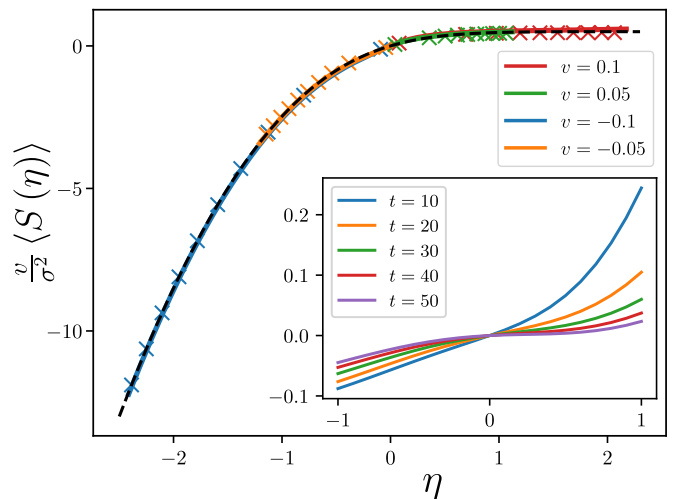


FIG. 3. Scaling limit for the discrete model (see Caption of Fig. 2) by solving Eq. (8) (crosses) and for the continuous-time model (full lines) by solving Eq. (11). In both cases, we compute $v/\sigma^2 \langle S \rangle$ as a function of $\eta = v/\sigma\sqrt{t}/2$, at times up to $t = 10^3$, for various values of v . Numerical results are compared to the theoretical scaling function $S(\eta)$ of Eq. (14) (black dashed line). Inset: The difference $v/\sigma^2 \langle S \rangle - S$ is shown, as a function of η for increasing times t .

coincides with the well-known freezing transition of the DP. This happens even though the MIPT is dominated by rare events and indeed the critical properties are different.

Several perspectives open up. From the practical standpoint of chaos mitigation, it would be of interest to analyze more optimized strategies where one tries to minimize the number of measurements to be taken while still pinpointing the state of the system. From the perspective of directed polymer, it would be interesting to assess whether the coincidence of the two critical points (MIPT and freezing) observed on the tree is a more general property. Additionally, while no transition is expected for a lattice in dimension $d = 1$ [64], the tree provides a good qualitative description for sufficiently high d (presumably for $d > 2$ when the polymer shows a high temperature phase and self-averaging properties [71, 72]).

ACKNOWLEDGEMENTS.

FG acknowledges support from Université Paris-Saclay. GG and ADL acknowledge support by the ANR JCJC grant ANR-21-CE47-0003 (TamEnt). PLD acknowledges support from ANR grant ANR-23-CE30-0020-01 EDIPS.

-
- [1] J. Preskill, Quantum Computing in the NISQ era and beyond, *Quantum* **2**, 79 (2018).
- [2] J. C. Hoke, M. Ippoliti, E. Rosenberg, D. Abanin, R. Acharya, T. I. Andersen, M. Ansmann, F. Arute, K. Arya, A. Asfaw, J. Atalaya, J. C. Bardin, A. Bengtsson, G. Bortoli, A. Bourassa, *et al.*, Measurement-induced entanglement and teleportation on a noisy quantum processor, *Nature* **622**, 481 (2023).
- [3] A. Nahum, S. Vijay, and J. Haah, Operator spreading in random unitary circuits, *Phys. Rev. X* **8**, 021014 (2018).
- [4] A. Christopoulos, P. Le Doussal, D. Bernard, and A. De Luca, Universal out-of-equilibrium dynamics of 1d critical quantum systems perturbed by noise coupled to energy, *Phys. Rev. X* **13**, 011043 (2023).
- [5] L. Hruza and D. Bernard, Coherent fluctuations in noisy mesoscopic systems, the open quantum ssep, and free probability, *Phys. Rev. X* **13**, 011045 (2023).
- [6] D. Bernard, Can the macroscopic fluctuation theory be quantized?, *Journal of Physics A: Mathematical and Theoretical* **54**, 433001 (2021).
- [7] S. Roy, J. T. Chalker, I. V. Gornyi, and Y. Gefen, Measurement-induced steering of quantum systems, *Phys. Rev. Res.* **2**, 033347 (2020).
- [8] O. Lunt, J. Richter, and A. Pal, Quantum simulation using noisy unitary circuits and measurements, in *Entanglement in Spin Chains: From Theory to Quantum Technology Applications*, edited by A. Bayat, S. Bose, and H. Johannesson (Springer, Cham, 2022) pp. 251–284.
- [9] T. Botzung, S. Diehl, and M. Müller, Engineered dissipation induced entanglement transition in quantum spin chains: From logarithmic growth to area law, *Phys. Rev. B* **104**, 184422 (2021).
- [10] C. M. Caves and G. J. Milburn, Quantum-mechanical model for continuous position measurements, *Phys. Rev. A* **36**, 5543 (1987).
- [11] L. D’Alessio, Y. Kafri, A. Polkovnikov, and M. Rigol, From quantum chaos and eigenstate thermalization to statistical mechanics and thermodynamics, *Advances in Physics* **65**, 239 (2016), <https://doi.org/10.1080/00018732.2016.1198134>.
- [12] D. A. Abanin, E. Altman, I. Bloch, and M. Serbyn, Colloquium: Many-body localization, thermalization, and entanglement, *Rev. Mod. Phys.* **91**, 021001 (2019).
- [13] A. Nahum, J. Ruhman, S. Vijay, and J. Haah, Quantum entanglement growth under random unitary dynamics, *Phys. Rev. X* **7**, 031016 (2017).
- [14] A. Chan, A. De Luca, and J. T. Chalker, Solution of a minimal model for many-body quantum chaos, *Phys. Rev. X* **8**, 041019 (2018).
- [15] B. Bertini, P. Kos, and T. c. v. Prosen, Entanglement spreading in a minimal model of maximal many-body quantum chaos, *Phys. Rev. X* **9**, 021033 (2019).
- [16] B. Skinner, J. Ruhman, and A. Nahum, Measurement-induced phase transitions in the dynamics of entanglement, *Phys. Rev. X* **9**, 031009 (2019).
- [17] Y. Li, X. Chen, and M. P. A. Fisher, Quantum zeno effect and the many-body entanglement transition, *Phys. Rev. B* **98**, 205136 (2018).
- [18] C.-M. Jian, Y.-Z. You, R. Vasseur, and A. W. W. Ludwig, Measurement-induced criticality in random quantum circuits, *Phys. Rev. B* **101**, 104302 (2020).
- [19] M. J. Gullans and D. A. Huse, Dynamical purification phase transition induced by quantum measurements, *Phys. Rev. X* **10**, 041020 (2020).
- [20] Y. Li, X. Chen, and M. P. A. Fisher, Measurement-driven entanglement transition in hybrid quantum circuits, *Phys. Rev. B* **100**, 134306 (2019).
- [21] S. Choi, Y. Bao, X.-L. Qi, and E. Altman, Quantum error correction in scrambling dynamics and measurement-induced phase transition, *Phys. Rev. Lett.* **125**, 030505 (2020).
- [22] R. Fan, S. Vijay, A. Vishwanath, and Y.-Z. You, Self-organized error correction in random unitary circuits with measurement, *Phys. Rev. B* **103**, 174309 (2021).
- [23] Y. Li and M. P. A. Fisher, Statistical mechanics of quantum error correcting codes, *Phys. Rev. B* **103**, 104306 (2021).
- [24] G. Vidal, Efficient classical simulation of slightly entangled quantum computations, *Phys. Rev. Lett.* **91**, 147902 (2003).
- [25] R. Vasseur, A. C. Potter, Y.-Z. You, and A. W. W. Ludwig, Entanglement transitions from holographic random tensor networks, *Phys. Rev. B* **100**, 134203 (2019).
- [26] M. Mézard, G. Parisi, and M. A. Virasoro, *Spin glass theory and beyond*, Vol. 9 (World Scientific Publishing Company, 1987).
- [27] A. J. Bray and M. A. Moore, Replica theory of quantum spin glasses, *Journal of Physics C: Solid State Physics* **13**, L655 (1980).
- [28] X. Cao, A. Tilloy, and A. De Luca, Entanglement in a fermion chain under continuous monitoring, *SciPost Phys.* **7**, 024 (2019).
- [29] M. Coppola, E. Tirrito, D. Karevski, and M. Collura, Growth of entanglement entropy under local projective measurements, *Phys. Rev. B* **105**, 094303 (2022).
- [30] O. Albertson, M. Buchhold, and S. Diehl, Entanglement transition in a monitored free-fermion chain: From extended criticality to area law, *Phys. Rev. Lett.* **126**, 170602 (2021).
- [31] M. Buchhold, Y. Minoguchi, A. Altland, and S. Diehl, Effective theory for the measurement-induced phase transition of dirac fermions, *Phys. Rev. X* **11**, 041004 (2021).
- [32] M. Lucas, L. Piroli, J. De Nardis, and A. De Luca, Generalized deep thermalization for free fermions, *Phys. Rev. A* **107**, 032215 (2023).
- [33] L. Fidkowski, J. Haah, and M. B. Hastings, How Dynamical Quantum Memories Forget, *Quantum* **5**, 382 (2021).
- [34] H. Lóio, A. De Luca, J. De Nardis, and X. Turkeshi, Purification timescales in monitored fermions, *Phys. Rev. B* **108**, L020306 (2023).
- [35] J. Merritt and L. Fidkowski, Entanglement transitions with free fermions, *Phys. Rev. B* **107**, 064303 (2023).
- [36] F. Evers and A. D. Mirlin, Anderson transitions, *Rev. Mod. Phys.* **80**, 1355 (2008).
- [37] M. Fava, L. Piroli, T. Swann, D. Bernard, and A. Nahum, Nonlinear sigma models for monitored dynamics of free fermions, *Phys. Rev. X* **13**, 041045 (2023).
- [38] I. Poboiko, P. Pöpperl, I. V. Gornyi, and A. D. Mirlin, Theory of free fermions under random projective measurements, *Phys. Rev. X* **13**, 041046 (2023).
- [39] S.-K. Jian, C. Liu, X. Chen, B. Swingle, and P. Zhang, Measurement-induced phase transition in the monitored sachdev-ye-kitaev model, *Phys. Rev. Lett.* **127**, 140601 (2021).

- [40] X. Turkeshi, M. Dalmonte, R. Fazio, and M. Schirò, Entanglement transitions from stochastic resetting of non-hermitian quasiparticles, *Phys. Rev. B* **105**, L241114 (2022).
- [41] X. Turkeshi, A. Biella, R. Fazio, M. Dalmonte, and M. Schirò, Measurement-induced entanglement transitions in the quantum ising chain: From infinite to zero clicks, *Phys. Rev. B* **103**, 224210 (2021).
- [42] Y. Bao, S. Choi, and E. Altman, Theory of the phase transition in random unitary circuits with measurements, *Phys. Rev. B* **101**, 104301 (2020).
- [43] A. Zabalo, M. J. Gullans, J. H. Wilson, S. Gopalakrishnan, D. A. Huse, and J. H. Pixley, Critical properties of the measurement-induced transition in random quantum circuits, *Phys. Rev. B* **101**, 060301 (2020).
- [44] P. Zhang, S.-K. Jian, C. Liu, and X. Chen, Emergent Replica Conformal Symmetry in Non-Hermitian SYK₂ Chains, *Quantum* **5**, 579 (2021).
- [45] A. Nahum, S. Roy, B. Skinner, and J. Ruhman, Measurement and entanglement phase transitions in all-to-all quantum circuits, on quantum trees, and in landauginsburg theory, *PRX Quantum* **2**, 010352 (2021).
- [46] G. S. Bentsen, S. Sahu, and B. Swingle, Measurement-induced purification in large-n hybrid brownian circuits, *Physical Review B* **104**, 094304 (2021).
- [47] J. Lopez-Piqueres, B. Ware, and R. Vasseur, Mean-field entanglement transitions in random tree tensor networks, *Phys. Rev. B* **102**, 064202 (2020).
- [48] A. De Luca, C. Liu, A. Nahum, and T. Zhou, Universality classes for purification in nonunitary quantum processes (2024), arXiv:2312.17744 [cond-mat.stat-mech].
- [49] F. Gerbino, P. Le Doussal, G. Giachetti, and A. De Luca, A dyson brownian motion model for weak measurements in chaotic quantum systems, *Quantum Reports* **6**, 200 (2024).
- [50] A. Zabalo, M. J. Gullans, J. H. Wilson, R. Vasseur, A. W. W. Ludwig, S. Gopalakrishnan, D. A. Huse, and J. H. Pixley, Operator scaling dimensions and multifractality at measurement-induced transitions, *Phys. Rev. Lett.* **128**, 050602 (2022).
- [51] A. Nahum and K. J. Wiese, Renormalization group for measurement and entanglement phase transitions, *Phys. Rev. B* **108**, 104203 (2023).
- [52] Y. Li, X. Chen, A. W. W. Ludwig, and M. P. A. Fisher, Conformal invariance and quantum nonlocality in critical hybrid circuits, *Phys. Rev. B* **104**, 104305 (2021).
- [53] Q. Tang and W. Zhu, Measurement-induced phase transition: A case study in the nonintegrable model by density-matrix renormalization group calculations, *Phys. Rev. Res.* **2**, 013022 (2020).
- [54] G. Cecile, H. Lóio, and J. De Nardis, Measurement-induced phase transitions by matrix product states scaling, *Phys. Rev. Res.* **6**, 033220 (2024).
- [55] Y. Li, R. Vasseur, M. P. A. Fisher, and A. W. W. Ludwig, Statistical mechanics model for clifford random tensor networks and monitored quantum circuits, *Phys. Rev. B* **109**, 174307 (2024).
- [56] X. Turkeshi, Measurement-induced criticality as a data-structure transition, *Phys. Rev. B* **106**, 144313 (2022).
- [57] J. M. Koh, S.-N. Sun, M. Motta, and A. J. Minnich, Measurement-induced entanglement phase transition on a superconducting quantum processor with mid-circuit readout, *Nature Physics* **19**, 1314 (2023).
- [58] S. Czischek, G. Torlai, S. Ray, R. Islam, and R. G. Melko, Simulating a measurement-induced phase transition for trapped-ion circuits, *Phys. Rev. A* **104**, 062405 (2021).
- [59] C. Noel, P. Niroula, D. Zhu, A. Risinger, L. Egan, D. Biswas, M. Cetina, A. V. Gorshkov, M. J. Gullans, D. A. Huse, and C. Monroe, Measurement-induced quantum phases realized in a trapped-ion quantum computer, *Nat. Phys.* **18**, 760 (2022).
- [60] M. J. Gullans and D. A. Huse, Scalable probes of measurement-induced criticality, *Phys. Rev. Lett.* **125**, 070606 (2020).
- [61] M. Ippoliti and V. Khemani, Postselection-free entanglement dynamics via spacetime duality, *Phys. Rev. Lett.* **126**, 060501 (2021).
- [62] J. Willsher, S.-W. Liu, R. Moessner, and J. Knolle, Measurement-induced phase transition in a chaotic classical many-body system, *Phys. Rev. B* **106**, 024305 (2022).
- [63] A. Pizzi, D. Malz, A. Nunnenkamp, and J. Knolle, Bridging the gap between classical and quantum many-body information dynamics, *Phys. Rev. B* **106**, 214303 (2022).
- [64] T. Jin and D. G. Martin, Kardar-parisi-zhang physics and phase transition in a classical single random walker under continuous measurement, *Phys. Rev. Lett.* **129**, 260603 (2022).
- [65] B. Derrida and H. Spohn, Polymers on disordered trees, spin glasses, and traveling waves, *Journal of Statistical Physics* **51**, 817 (1988).
- [66] D. Carpentier and P. Le Doussal, Glass transition of a particle in a random potential, front selection in nonlinear renormalization group, and entropic phenomena in liouville and sinh-gordon models, *Physical review E* **63**, 026110 (2001).
- [67] G. Giachetti and A. De Luca, Elusive phase transition in the replica limit of monitored systems (2023), arXiv:2306.12166 [cond-mat.stat-mech].
- [68] See Supplemental Material for additional details.
- [69] In the language of directed polymer, the chemical potential and inverse temperature are proportional to the mean and to the r.m.s of $\ln P_1(a)/(KP_0(a))$ respectively.
- [70] As obtained by linearizing (10) for $h_t(y) \ll 1$ [65]. Here $v_{\text{KPP}} = \lim_{t \rightarrow +\infty} \frac{1}{t} \log Z^{(\tau)}$ is the intensive free energy associated to typical polymer paths (i.e. $n = 0$). $v_{\text{KPP}} = 0$ corresponds to the high-T phase with $\bar{h}(z) \sim e^{-z}$, $\alpha = 0$, and $\sigma > \sqrt{2\lambda}$ to the low-T phase with $\bar{h}(z) \sim e^{-\sqrt{2\lambda}z/\sigma}$ for $z \gg 1$ and $\alpha = 3/4$. At the transition $\alpha = 1/4$.
- [71] T. Halpin-Healy and Y.-C. Zhang, Kinetic roughening phenomena, stochastic growth, directed polymers and all that. aspects of multidisciplinary statistical mechanics, *Physics reports* **254**, 215 (1995).
- [72] F. Comets *et al.*, *Directed polymers in random environments* (Springer, 2017).
- [73] C. Gardiner, *Handbook of Stochastic Methods for Physics, Chemistry, and the Natural Sciences*, Proceedings in Life Sciences (Springer-Verlag, 1985).
- [74] It is also $U_T(Y) = \text{Prob}(\min_{0 \leq \tau \leq T} X(\tau) > 0)$ for a Wiener process of drift $-\xi$ with $X(0) = Y$.

End Matter

Appendix A: One-point contribution to $\langle S_t \rangle$

We will now compute the one-point contribution to $\langle S_t \rangle$, i.e., the second term in the r.h.s. of Eq. (5). This can be rewritten in terms of replicas as

$$\sum_{j=1}^{K^\tau} \langle z_j^{(\tau)} \ln z_j^{(\tau)} \rangle_0 = \partial_n \sum_{j=1}^{K^\tau} \langle (z_j^{(\tau)})^n \rangle_0 \Big|_{n=1}, \quad (\text{SA.1})$$

while, according to our definition of the z_j

$$z_j^{(\tau)} = \prod_{p \in \text{branch}} \frac{P_1(a_p)}{K P_0(a_p)}, \quad (\text{SA.2})$$

where the product runs over the tree branch that connects site j to the origin. As all the a_p are independent one has

$$\sum_{j=1}^{K^\tau} \langle (z_j^{(\tau)})^n \rangle_0 = K^{-(n-1)\tau} \left\langle \left(\frac{P_1(a)}{P_0(a)} \right)^{n-1} \right\rangle_1 \quad (\text{SA.3})$$

where we made use of the fact that $\langle (P_1(a)/P_0(a))^n \rangle_0 = \langle (P_1(a)/P_0(a))^{n-1} \rangle_1$. Finally, by taking the derivative we find

$$\sum_{j=1}^{K^\tau} \langle z_j^{(\tau)} \ln z_j^{(\tau)} \rangle_0 = \tau (D_{\text{KL}}(P_1 \parallel P_0) - \ln K). \quad (\text{SA.4})$$

Appendix B: Proof of Eq. (9)

We want now to estimate the collective contribution to $\langle S_t \rangle$, i.e. the first term in the r.h.s. of Eq. (5). First, we express it in terms of $G_\tau(y)$. To do so we notice that, integrating twice in Z both sides of the identity

$$Z^{-1} = \int_0^{+\infty} ds e^{-sZ} \quad (\text{SB.1})$$

we get

$$Z \ln Z = \int_0^\infty \frac{ds}{s^2} (e^{-sZ} - e^{-s} + (Z-1)e^{-s}s(s+1)) \quad (\text{SB.2})$$

Let us now set $Z = Z^{(\tau)}$, $s = e^{-y}$ and take the average of both sides: by taking into account the fact that $\langle Z^{(\tau)} \rangle_0 = 1$ and $G_0(y) = e^{-e^{-y}}$, we get

$$\langle Z^{(\tau)} \ln Z^{(\tau)} \rangle_0 = \int_{-\infty}^\infty dy e^y (G_\tau(y) - G_0(y)). \quad (\text{SB.3})$$

that, expressed in terms of $u_\tau(y) = e^{-y}(1 - G_\tau(y))$ gives Eq. (9).

Appendix C: Discrete-time case

We will show that we can recover the linearized form of Eq. (11) without the assumption of small Δt , in the regime $\tau \gg 1$. Indeed, by expressing the discrete recursion relation Eq. (8) in terms of $u_\tau(y) = e^y(1 - G_\tau(y))$ and expanding to the leading order in $u_\tau(y)e^{-y}$ we get

$$u_{\tau+1}(y) = \left\langle u_\tau \left(y + \ln K - \ln \frac{P_1(a)}{P_0(a)} \right) \right\rangle_1, \quad (\text{SC.1})$$

where now $u_0(y) = e^y(1 - e^{-e^{-y}})$. The solution can thus be expressed as

$$u_\tau(y) = \int dy' \mathcal{U}_\tau(y') u_0(y + y') \quad (\text{SC.2})$$

where $\mathcal{U}_\tau(y)$ is the Green's function associated to Eq. (SC.1). The latter can in turn be expressed in terms of Fourier modes as

$$\mathcal{U}_\tau(y) = \int \frac{dq}{2\pi} e^{iqy + \omega(q)\tau} \quad (\text{SC.3})$$

with $\omega(q) = iq \ln K + \ln \langle e^{-iq \ln P_1(a)/P_0(a)} \rangle_1$. We now want to evaluate the latter expression in the large-time limit. Setting $q \rightarrow q/\sqrt{\tau}$, only the first two orders in q of $\omega(q)$ contribute: as $\omega(q) = -iqv\Delta t - \text{Var}(P_1 \parallel P_0)q^2/2 + O(q^3)$ we see that, for any $t = \tau\Delta t$

$$\mathcal{U}_\tau(y) = \frac{e^{-(y-vt)^2/(2\sigma^2t)}}{\sqrt{2\pi\sigma^2t}} + O(\tau^{-1}), \quad (\text{SC.4})$$

and

$$u_\tau(y) = \int \frac{dy'}{\sqrt{2\pi\sigma^2t}} e^{-(y-vt)^2/(2\sigma^2t)} u_0(y + y'), \quad (\text{SC.5})$$

that provides the general solution of Eq. (11) in the linear regime.

Appendix D: Continuum limit

To properly define the continuum limit, one has to take $P_0(a) - P_1(a) \sim O(\sqrt{\Delta t})$, namely

$$P_0(a) = P_1(a) + \pi_1(a)\sqrt{\Delta t} + \pi_2(a)\Delta t + O(\Delta t)^{3/2} \quad (\text{SD.1})$$

where the normalization requires $\int \pi_{1,2}(a) = 0$. From this one has, up to terms $O(\Delta t)^{3/2}$

$$\ln \frac{P_1(a)}{P_0(a)} = -\frac{\pi_1(a)}{P_1(a)}\sqrt{\Delta t} + \left(\frac{1}{2} \frac{\pi_1^2(a)}{P_1^2(a)} - \frac{\pi_2(a)}{P_1(a)} \right) \Delta t. \quad (\text{SD.2})$$

Taking the average of (SD.2) w.r.t. P_1 gives, at leading order

$$D_{\text{KL}}(P_1 \parallel P_0) \simeq \frac{\Delta t}{2} \int da \frac{\pi_1^2(a)}{P_1(a)} := \frac{\sigma^2}{2} \Delta t, \quad (\text{SD.3})$$

while taking the variance of (SD.2) w.r.t. P_1 gives

$$\begin{aligned} \text{Var}(P_1 \parallel P_0) &= \text{Var}(P_0 \parallel P_1) \quad (\text{SD.4}) \\ &= \langle \ln^2(P_1(a)/P_0(a)) \rangle_1 - \langle \ln(P_1(a)/P_0(a)) \rangle_1^2 \\ &= \Delta t \int da \frac{\pi_1^2(a)}{P_1(a)} + o(\Delta t) = 2D_{\text{KL}}(P_1 \parallel P_0) + o(\Delta t), \end{aligned}$$

which is the relation presented in the main text, with $\text{Var}(P_1 \parallel P_0) = \sigma^2 \Delta t$.

Note that to obtain Eq. (10) we also used that, to leading order

$$\left\langle \ln \frac{P_1(a)}{P_0(a)} \right\rangle_0 \simeq -\Delta t \int da \frac{\pi_1^2(a)}{P_1(a)} = -\frac{\sigma^2}{2} \Delta t. \quad (\text{SD.5})$$

Appendix E: Rate of entropy production

From Eq. (5) and (9), one has the exact relation

$$\partial_t \langle S_t \rangle = -v - \int_{-\infty}^{+\infty} dy \partial_t u_t(y), \quad (\text{SE.1})$$

Using (11) and integrating over $y \in (-\infty, \infty)$ using that $u_t(y)$ vanishes at $y = -\infty$ and tends to 1 at $y = +\infty$, one finds another exact relation for the entropy production at time t

$$\partial_t \langle S_t \rangle = \lambda \int_{-\infty}^{+\infty} dy e^y \tilde{F}(e^{-y} u_t(y)). \quad (\text{SE.2})$$

One can check that $h^2/2 < \tilde{F}(h) < h^2$. Hence one needs to evaluate $A_t = \int_{-\infty}^{+\infty} dy e^{-y} u_t(y)^2 = \int_{-\infty}^{+\infty} dy e^y h_t(y)^2$. This is always a convergent integral since $h_t(y) \rightarrow 1$ for $y \rightarrow -\infty$ and $h_t(y) \sim e^{-y}$ for $y \rightarrow +\infty$. For $v > 0$ the KPP front solution $h_t(y) = \tilde{h}(y - y_t)$ has a strictly negative velocity, which implies that on $[y_0, +\infty)$ for any y_0 one has that $h_t(y) \rightarrow 0$. Hence for $v > 0$, $A_t \rightarrow 0$ and the rate of entropy production vanishes $s = 0$. More precisely one finds that for $\sqrt{2\lambda} < \sigma < 2\sqrt{2\lambda}$ the decay of A_t is dominated by the KPP front with $A_t \rightarrow e^{v t} \int dz e^z \tilde{h}(z)^2 \sim e^{-|v_{\text{KPP}}|t}$, while for $\sigma > 2\sqrt{2\lambda}$ it is dominated by the far tail of $h_t(y)$. For $v = 0$ the KPP front moves more slowly to the left, $y_t \simeq -\frac{1}{2} \ln t$ (see Sec. I) leading to slower decay of $A_t \sim 1/\sqrt{t}$, consistent with the results in the main text.

Appendix F: Critical scaling

By setting $y = \sigma^2 Y/|v|$, $t = \sigma^2 T/v^2$, Eq. (11) becomes, for $U_T(Y) = u_t(y)$ with $Y, T = O(1)$:

$$\partial_T U_T(Y) = -\xi \partial_Y U_T(Y) + \frac{1}{2} \partial_Y^2 U_T(Y) + \dots, \quad (\text{SF.1})$$

with $\xi = \text{sign}(v)$ and $U_T(+\infty) = 1$. The non linear part ... reads $\frac{\sigma^2}{v^2} e^{\sigma^2 Y/|v|} \tilde{F}(e^{-\sigma^2 Y/|v|} U_T(Y))$. As explained in

the text, it can be neglected for $Y > 0$, while it acts as a wall imposing $U_T(Y \leq 0) = 0$. Thus, Eq. (SF.1) is the evolution equation for the cumulative probability density of a Wiener process on $Y > 0$, with drift velocity ξ , and a reflecting boundary wall at $Y = 0$. Taking as initial condition $U_{T=0}(Y) = \theta(Y)$, the solution of this problem can be written as a Galilean transformation of the $\xi = 0$ solution obtained through the reflection principle[73], namely [74]

$$U_T(Y) = \Phi\left(\frac{Y - \xi T}{\sqrt{2T}}\right) - e^{2\xi Y} \left[1 - \Phi\left(\frac{Y + \xi T}{\sqrt{2T}}\right)\right], \quad (\text{SF.2})$$

where $\Phi(x) = (1 + \text{erf}(x))/2$ is the cumulative of the Gaussian distribution with variance 1/2.

To compute the entropy, we use (SE.1). Recalling that $t = \sigma^2 T/v^2$ and $y = \sigma^2 Y/|v|$, this leads to

$$\frac{|v|}{\sigma^2} \partial_T \langle S_T \rangle = -\xi - \int_0^{+\infty} dY \partial_T U_T(Y) = \frac{1}{2} \partial_Y U_T(Y)|_{Y=0}$$

implying that

$$\frac{v}{\sigma^2} \partial_T \langle S_T \rangle = \frac{e^{-\frac{\xi}{2}}}{\sqrt{2\pi\xi\sqrt{T}}} - \frac{1}{2} \text{erfc}\left(\frac{\xi\sqrt{T}}{\sqrt{2}}\right) \quad (\text{SF.3})$$

which, integrated over time gives Eq. (13) with the scaling function (14) with $\eta = \xi\sqrt{T}/2$, which is analytic in η .

Although this derivation was carried out in the continuous model, let us notice that it is possible to retrieve the same result in the discrete-time case $\Delta t = O(1)$ as well. Indeed, rescaling $t = \tau \Delta t = T \sigma^2/v^2$ the variable $T = O(1)$ is naturally continuous via the simultaneous limit $\tau \rightarrow \infty$, $v \rightarrow 0$. Namely, finite increments $\tau \rightarrow \tau + 1$ correspond to infinitesimal increments $T \rightarrow T + v^2/\sigma^2$.

SUPPLEMENTAL MATERIAL

Monitoring of a single diffusive particle with replica trick

Appendix G: Averaging over realizations of the physical particle

In the main text we have formulated our model as follows

- A single particle undergoes a directed diffusion on the Cayley tree and we denote as $x_\tau \in \{1, \dots, K^\tau\}$ its position at each time;
- At each time-step τ and each site $j = 1, \dots, K^\tau$ a measurement is performed resulting in a measurement outcome $a_j^{(\tau)}$ distributed according to $P(a_j|x) := P_{\delta_{j,x}}(a)$ (to clarify the notation, we use $\mathbf{a}^{(\tau)}$ to denote the outcomes of measurements at time-step τ , while $\mathbf{a}^{(\leq \tau)}$ denotes the collection of all measurement outcomes up to time τ);
- the observer uses the knowledge of all a 's up to time τ to update with Bayes' theorem their knowledge of the location of the particle which results in the probabilities $p_j^{(\tau)} = P(j^{(\tau)}|\mathbf{a}^{(\leq \tau)})$ that $x_\tau = j$.

We are then interested in computing averages over the realizations of the trajectory of the particle of functionals $\langle F(\mathbf{p}^{(\tau)}) \rangle_x$ of the probabilities assigned by the observer at a given time τ . We will now show that one can practically disregard the evolution of the physical particle and use (2) and (3) to evolve the probabilities \mathbf{p} and the measurement outcomes \mathbf{a} . Since we are dealing with the Cayley tree, we note that there is a unique trajectory ending on each leaf labeled by $x_\tau = 1, \dots, K^\tau$. Given the realization x_τ , the probabilities of the a 's factorizes

$$P(\mathbf{a}^{(\leq \tau)}|x_\tau) = \prod_{\tau' \leq \tau} \prod_{j=1}^{K^{\tau'}} p(a_j^{(\tau')}|x_{\tau'}). \quad (\text{SG.1})$$

Also, from the knowledge of the $a^{(\tau+1)}$ and of the previous set of probabilities $\mathbf{p}^{(\tau)}$, the observer can compute the probabilities at time $\tau + 1$ from Eq. (2), which we can compactly rewrite as

$$P(j^{(\tau+1)}|\mathbf{a}^{(\tau+1)}, \mathbf{p}^{(\tau)}) := \omega_j(\mathbf{p}^{(\tau)}, \mathbf{a}^{(\tau+1)}). \quad (\text{SG.2})$$

Iterating this equation, one can express explicitly the probability assigned by the observer given all the measurement outcomes $\mathbf{a}^{(\leq \tau)}$

$$P(j^{(\tau)}|\mathbf{a}^{(\leq \tau)}) := \omega_j(\omega(\dots \omega(\mathbf{p}^{(0)}, \mathbf{a}^{(1)}), \mathbf{a}^{(2)}) \dots \mathbf{a}^{(\tau)}) = \dots =: \Omega_j(\mathbf{a}^{(\leq \tau)}), \quad (\text{SG.3})$$

which defines implicitly the function Ω of all the measurement outcomes at all times $\leq \tau$. By Bayes' theorem, one can also write this more explicitly as

$$\Omega_j(\mathbf{a}^{(\leq \tau)}) = \frac{P(\mathbf{a}^{(\leq \tau)}|j^{(\tau)})}{\sum_{j'=1}^{K^\tau} P(\mathbf{a}^{(\leq \tau)}|j'^{(\tau)})}. \quad (\text{SG.4})$$

Combining (SG.1) and (SG.3), we can write the probability distribution for the p_j 's assigned by the observer given a realization of the particle

$$P(\mathbf{p}^{(\tau)}|x_\tau) := \int d\mathbf{a}^{(\leq \tau)} \delta(\mathbf{p}^{(\tau)} - \Omega(\mathbf{a}^{(\leq \tau)})) P(\mathbf{a}^{(\leq \tau)}|x_\tau). \quad (\text{SG.5})$$

Then, averaging over all trajectories of the physical particle, we get the distribution we are interested in

$$P(\mathbf{p}^{(\tau)}) = \frac{1}{K^\tau} \sum_{x_\tau} P(\mathbf{p}^{(\tau)}|x_\tau). \quad (\text{SG.6})$$

Using Eq. (SG.3) and (SG.4), we obtain that

$$P(\mathbf{p}^{(\tau)}|x_\tau) := p_{x_\tau}^{(\tau)} \int d\mathbf{a}^{(\leq \tau)} \delta(\mathbf{p}^{(\tau)} - \Omega(\mathbf{a}^{(\leq \tau)})) \sum_{j'} P(\mathbf{a}^{(\leq \tau)}|j'^{(\tau)}) = K^\tau p_{x_\tau}^{(\tau)} P(\mathbf{p}^{(\tau)}) \quad (\text{SG.7})$$

We can now show that Eq. (SG.6) admits a recursive representation. Indeed,

$$\begin{aligned}
P(\mathbf{p}^{(\tau+1)}) &= \frac{1}{K^{\tau+1}} \sum_{x^{(\tau+1)}} \int d\mathbf{a}^{(\leq\tau+1)} \delta(\mathbf{p}^{(\tau+1)} - \Omega(\mathbf{a}^{(\leq\tau+1)})) P(\mathbf{a}^{(\leq\tau+1)} | x^{(\tau+1)}) = \\
&= \frac{1}{K^{\tau+1}} \sum_{x^{(\tau+1)}} \int d\mathbf{a}^{(\tau+1)} \int d\mathbf{p}^{(\tau)} \delta(\mathbf{p}^{(\tau+1)} - \omega(\mathbf{p}^{(\tau)}, \mathbf{a}^{(\tau+1)})) P(\mathbf{a}^{(\tau+1)} | x^{(\tau+1)}) \times \\
&= \int d\mathbf{a}^{(\leq\tau)} \delta(\mathbf{p}^{(\tau)} - \Omega(\mathbf{a}^{(\leq\tau)})) P(\mathbf{a}^{(\leq\tau)} | x^{(\tau+1)}) \quad (\text{SG.8})
\end{aligned}$$

Now, the end point $x^{(\tau+1)}$ fixes also the trajectory at x_τ and in the last line we recognise (SG.5). Thus from Eq. (SG.7), we arrive at

$$P(\mathbf{p}^{(\tau+1)}) = \int d\mathbf{a}^{(\tau+1)} \int d\mathbf{p}^{(\tau)} \delta(\mathbf{p}^{(\tau+1)} - \omega(\mathbf{p}^{(\tau)}, \mathbf{a}^{(\tau+1)})) P(\mathbf{p}^{(\tau)}) \sum_{x^{(\tau+1)}} P(\mathbf{a}^{(\tau+1)} | x^{(\tau+1)}) \frac{p_{x_\tau}}{K} \quad (\text{SG.9})$$

and using that $p_{x_\tau}^{(\tau)}/K = p_{x^{(\tau+1)}}^{(\tau+1,-)}$, we obtain precisely that the p_j can be evolved combining (2) and (3).

Appendix H: Equivalence of the two averages

In the main text, we have expressed the probability distribution $P(\mathbf{a}^{(\tau)} | \mathbf{p}^{(\tau,-)})$ of measurement outcomes $\mathbf{a}^{(\tau)}$ at time-step τ , conditioned on the probabilities $\mathbf{p}^{(\tau,-)}$ before measurements (c.f. Eq. (3)). We now show that the same quantity can be written in terms of the unnormalized variables $\mathbf{z}^{(\tau,-)}$. Starting from Eq. (3) one has

$$P(\mathbf{a}^{(\tau)} | \mathbf{p}^{(\tau,-)}) = \sum_{j=1}^{K^\tau} P(\mathbf{a}^{(\tau)} | j) p_j^{(\tau,-)} = \sum_{j=1}^{K^\tau} P(\mathbf{a}^{(\tau)} | j) \frac{z_j^{\tau,-}}{\sum_{j'=1}^{K^\tau} z_{j'}^{\tau,-}}. \quad (\text{SH.1})$$

Then, exploiting the fact that

$$\sum_{j'=1}^{K^\tau} z_{j'}^{\tau,-} = \sum_{j'=1}^{K^\tau} \frac{z_{[j'/K]}^{\tau-1}}{K} = K \sum_{j=1}^{K^{\tau-1}} \frac{z_j^{\tau-1}}{K} = Z^{(\tau-1)}, \quad (\text{SH.2})$$

inserting the definition for $P(\mathbf{a}^{(\tau)} | j)$ (Eq. (1) of the main text) and using that $P_1(a_j^{(\tau+1)})/P_0(a_j^{(\tau+1)})z_j^{(\tau,-)} = z_j^{(\tau)}$, one finds the simpler expression:

$$\sum_{j=1}^{K^\tau} P(\mathbf{a}^{(\tau)} | j) \frac{z_j^{\tau,-}}{\sum_{j'=1}^{K^\tau} z_{j'}^{\tau,-}} = \frac{\prod_{j=1}^{K^\tau} P_0(a_j^{(\tau)})}{Z^{(\tau-1)}} \sum_{j=1}^{K^\tau} \frac{P_1(a_j^{(\tau)})}{P_0(a_j^{(\tau)})} z_j^{\tau,-} = \frac{Z^{(\tau)}}{Z^{(\tau-1)}} \prod_{j=1}^{K^\tau} P_0(a_j^{(\tau)}), \quad (\text{SH.3})$$

where the last term $\prod_{j=1}^{K^\tau} P_0(a_j^{(\tau)})$ is the probability distribution for the unbiased process where all $a_j^{(\tau)}$ are independent with distribution $P_0(a)$. Let us notice that the ratio $Z^{(\tau)}/Z^{(\tau-1)}$ factorizes at each τ . Therefore, when taking products of distributions $P(\mathbf{a}^{(\tau')} | \mathbf{p}^{(\tau',-)})$ at increasing time-steps $1 \leq \tau' \leq \tau$, only $Z^{(0)} = 1$ and $Z^{(\tau)}$ do not cancel out, yielding:

$$\prod_{\tau'=1}^{\tau} P(\mathbf{a}^{(\tau')} | \mathbf{p}^{(\tau',-)}) = Z^{(\tau)} \prod_{\tau'=1}^{\tau} \left(\prod_{j=1}^{K^{\tau'}} P_0(a_j^{(\tau')}) \right). \quad (\text{SH.4})$$

The product in the above line corresponds exactly to the probability distribution of the full set of outcomes $\mathbf{a}^{(\leq\tau)}$. Finally, expressing functionals of probabilities $F[\{\mathbf{p}^{(\tau)}\}]$ as functionals of the $\mathbf{z}^{(\tau)}$, from (SH.4) one precisely obtains the equivalence between the two averages in Eq. (4) of the main text, namely:

$$\begin{aligned}
\langle F[\{\mathbf{p}^{(\tau)}\}] \rangle &= \int d\mathbf{a}^{(\leq\tau)} \prod_{\tau'=1}^{\tau} P(\mathbf{a}^{(\tau')} | \mathbf{p}^{(\tau',-)}) F[\{\mathbf{p}^{(\tau)}\}] = \\
&= \int d\mathbf{a}^{(\leq\tau)} \prod_{\tau'=1}^{\tau} \left(\prod_{j=1}^{K^{\tau'}} P_0(a_j^{(\tau')}) \right) F \left[\left\{ \frac{z_j^{(\tau)}}{Z^{(\tau)}} \right\} \right] Z^{(\tau)} = \left\langle F \left[\left\{ \frac{z_j^{(\tau)}}{Z^{(\tau)}} \right\} \right] Z^{(\tau)} \right\rangle_0. \quad (\text{SH.5})
\end{aligned}$$

Appendix I: Recall some details on the properties of the KPP equation

1. Velocity of the front

Consider the continuum model (10). The front velocity is obtained as follows [65]. One inserts $h_t(y) \simeq \bar{h}(z = y - y_t)$, assuming $\lim_{t \rightarrow +\infty} \frac{d}{dt} y_t = v_{\text{KPP}}$ in (10) leading to

$$0 = \frac{\sigma^2}{2} \bar{h}''(z) + (v_{\text{KPP}} + \lambda + \frac{\sigma^2}{2}) \bar{h}'(z) + \lambda F(\bar{h}(z)) \quad (\text{SI.1})$$

which determines $\bar{h}(z)$ if v_{KPP} is known. One then focuses on the forward region $z \gg 1$, inserting $\bar{h}(z) \sim e^{-\mu z}$ to linear order one finds the equation which determines v_{KPP} as a function of μ

$$\tilde{v}_{\text{KPP}} = v_{\text{KPP}} + \lambda + \frac{\sigma^2}{2} = \frac{\sigma^2}{2} \mu + \frac{\lambda}{\mu} \quad (\text{SI.2})$$

This parabola has a minimum at $\mu = \mu_c = \sqrt{2\lambda}/\sigma$. Since the initial condition decays as $h_0(y) \sim e^{-y}$ for $y \rightarrow +\infty$ one finds that

$$\begin{aligned} \sigma < \sqrt{2\lambda} \quad , \quad \mu = 1 \quad , \quad v_{\text{KPP}} = 0 \\ \sigma > \sqrt{2\lambda} \quad , \quad \mu = \mu_c \quad , \quad v_{\text{KPP}} = -(\sqrt{\lambda} - \frac{\sigma}{\sqrt{2}})^2 \end{aligned} \quad (\text{SI.3})$$

Here $v_{\text{KPP}} = \lim_{t \rightarrow +\infty} \frac{1}{t} \ln Z^{(\tau)}$ is the intensive free energy associated to typical polymer paths (i.e. $n = 0$). The first line corresponds to the high temperature phase of the directed polymer and the second to the low temperature phase where the front velocity is frozen (more precisely it is \tilde{v}_{KPP} which freezes to which one must add the drift $-(\lambda + \frac{\sigma^2}{2})$, which corresponds to an additional energy cost proportional to the polymer length. More precisely one has, following [65]

- (i) for $\sigma < \sqrt{2\lambda}$, $y_t \simeq O(1)$ and the KPP front decays as $\bar{h}(z) \sim e^{-z}$
- (ii) for $\sigma > \sqrt{2\lambda}$, $y_t \simeq v_{\text{KPP}} t - \frac{\alpha}{\lambda} \tilde{v}_{\text{KPP}} \ln(\lambda t) + O(1)$ where $\tilde{v}_{\text{KPP}} = \sigma \sqrt{2\lambda}$, with $\alpha = 3/4$, and $\bar{h}(z) \sim z e^{-\mu_c z}$ for $z \gg 1$ with $\mu_c = \sqrt{2\lambda}/\sigma$. At the transition $\sigma = \sqrt{2\lambda}$ the same holds with $\alpha = 1/4$ leading to $y_t \simeq -\frac{1}{2} \ln t + O(1)$.

2. Discrete model

Consider now the discrete time model. The linearized form of the recursion Eq. (8) with $G_\tau(y) = 1 - h_\tau(y)$ reads

$$h_{\tau+1}(y) = K \langle h_\tau(y - B(a)) \rangle_0, \quad (\text{SI.4})$$

where $B(a) = -\ln K + \ln \frac{P_1(a)}{P_0(a)}$. Looking for a front solution $h_\tau(y) = \bar{h}(y - c\tau)$ with $\bar{h}(z) \sim e^{-\mu z}$ we find

$$c = c(\mu) = \frac{1}{\mu} \ln \left(\left\langle K e^{\mu B(a)} \right\rangle_0 \right) \quad (\text{SI.5})$$

In the high temperature phase of the polymer $\mu = 1$ and

$$v_{\text{KPP}} = \frac{c(1)}{\Delta t} = \frac{1}{\Delta t} \ln \left(\left\langle K e^{B(a)} \right\rangle_0 \right) = 0 \quad (\text{SI.6})$$

In the low temperature phase of the polymer the front velocity and the parameter $\mu = \mu_c$ are determined by the conditions

$$v_{\text{KPP}} = c(\mu_c) = \frac{1}{\mu_c} \ln \left(\left\langle K e^{\mu_c B(a)} \right\rangle_0 \right) \quad (\text{SI.7})$$

$$\partial_\mu c(\mu)|_{\mu=\mu_c} = 0 \quad (\text{SI.8})$$

more precisely μ_c realizes the minimum of the function $c(\mu)$. The transition occurs when $\mu_c = 1$ and one can check that it corresponds to

$$-\ln K + \left\langle \frac{P_1(a)}{P_0(a)} \ln \frac{P_1(a)}{P_0(a)} \right\rangle_0 = v \Delta t = 0 \quad (\text{SI.9})$$

Thus it is a general property that the entropy rate transition occurs at the same location as the freezing transition of the directed polymer.

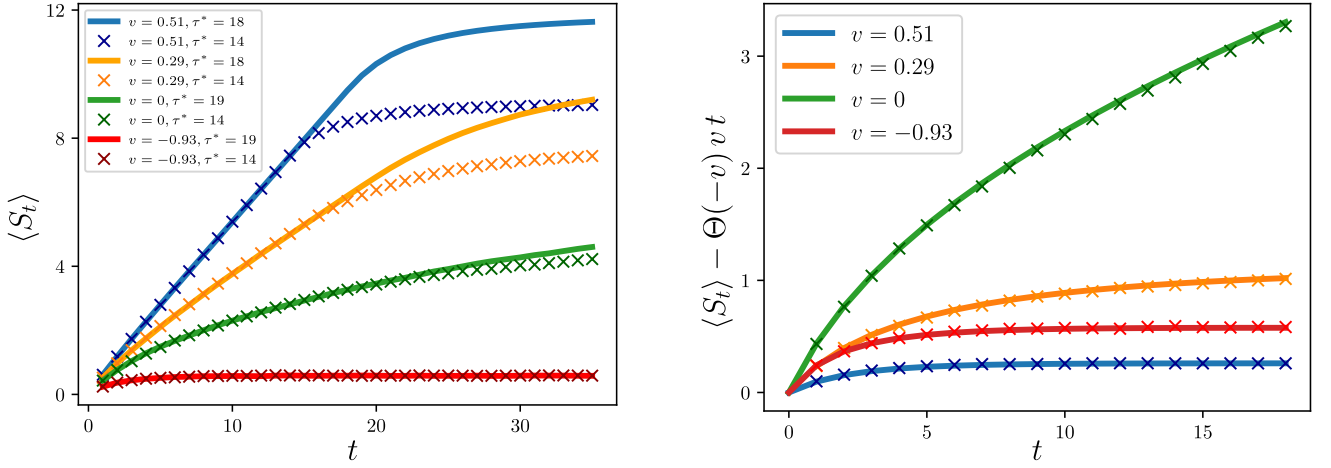


FIG. S1. (*Left:*) averaged entropy $\langle S_t \rangle$, for various values of the control parameter v . Trajectories are obtained evolving the biased probabilities \mathbf{p} . For small truncation times τ^* and $\epsilon < \epsilon_c$, the entropy $\langle S_t \rangle$ saturates to a value $\sim \tau^*$. Conversely, when $\epsilon > \epsilon_c$, the entropy $\langle S_t \rangle$ can be computed exactly at all times, independently on the value of τ^* . (*Right:*) finite contributions to the entropy $\langle S_t \rangle$. For negative values of v , we subtract the leading terms $\sim |v|t$. Markers represent data from simulations of the exact dynamics, while full lines are obtained via numerical solutions of Eq. (SK.1). The curves show good agreement between the two numerical approaches and the analytical results presented in the main text.

Appendix J: Weak noise expansion

In the weak noise/high temperature phase, i.e. $v < 0$, $\sigma < \sqrt{2\lambda}$, the solution of the KPP equation converges at large time to a limit, $h_t(y) \rightarrow h_\infty(y)$. One can compute this limit in a systematic weak noise/high temperature expansion. Setting $z = e^{-y}$, we look for a stationary solution of (10) (i.e. setting $\partial_t h_t(y) = 0$ there) in the form,

$$h_\infty(y) = 1 - e^{-z} - Q(z)e^{-z}, \quad Q(z) = \sum_{n \geq 1} \sigma^{2n} Q_n(z), \quad (\text{SJ.1})$$

where the coefficients, which must obey $Q_n(z) = O(z^2)$ for small z , are found as polynomials in z . Inserting (SJ.1) into (10) one finds

$$Q(z) = \frac{\sigma^2 z^2}{2\lambda} + \frac{\sigma^4 (z-2)^2 z^2}{8\lambda^2} + \frac{\sigma^6 (z-2)z^2((z-6)(z-4)z-12)}{48\lambda^3} + O(\sigma^8), \quad (\text{SJ.2})$$

leading to

$$\lim_{t \rightarrow +\infty} (\langle S_t \rangle + vt) = \lim_{\tau \rightarrow +\infty} \langle Z^{(\tau)} \ln Z^{(\tau)} \rangle_0 = \int_0^{+\infty} \frac{dz}{z^2} Q(z) e^{-z} = \frac{\sigma^2}{2\lambda} + \frac{\sigma^4}{4\lambda^2} + \frac{\sigma^6}{12\lambda^3} + O(\sigma^8). \quad (\text{SJ.3})$$

Appendix K: Numerical simulations

In this Section, we provide details about the numerics presented in the main text.

1. Montecarlo dynamics of the particle on the tree

First, we carry out simulations of the physical single-particle hopping process on a binary Cayley tree $K = 2$, choosing $P_0 \sim \mathcal{N}(0, 1)$ a Gaussian distribution, and $P_1 \sim \mathcal{N}(\epsilon, 1)$ a shifted Gaussian averaging to ϵ . With this choice of the probability distributions our control parameter becomes $v = D_{\text{KL}}(P_1 \parallel P_0) - \ln K = \epsilon^2/2 - \ln 2$, and the critical value of ϵ corresponding to $v = 0$ is then $\epsilon_c = \sqrt{2 \ln 2}$. We follow two equivalent approaches:

1. We can pick a random trajectory x_τ uniformly distributed among all those on the tree. Accordingly, we can determine the probability distribution for the measurement outcomes $\mathfrak{a}^{(\tau)}$ simply using the conditional

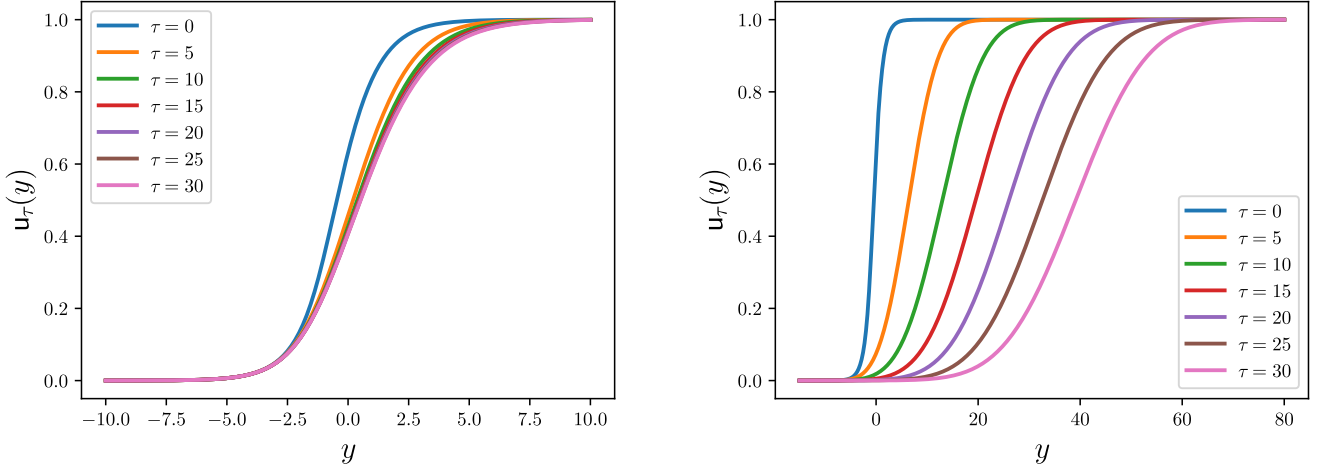


FIG. S2. Comparison between the evolved $u_\tau(y)$ for $v = -0.3$ (left) and $v = 1.3$ (right). In the former case, $u_\tau(y)$ freezes around a limiting shape, whereas in the latter case $u_\tau(y)$ is a wavefront moving rightwards with velocity v .

probability rule Eq. (1) of the main text. Since all physical trajectories are statistically equivalent, we can evolve $p_j^{(\tau)}$ considering $x_\tau = 0 \forall \tau$.

- Alternatively, as explained in the main text and in Sec. G, we can use Eq. (3) to generate the measurement outcomes $\mathbf{a}^{(\tau)}$ from the known probabilities $\mathbf{p}^{(\tau)}$ and Eq. (2) to consequently update the probabilities $\mathbf{p}^{(\tau)} \rightarrow \mathbf{p}^{(\tau+1)}$ themselves.

As a benchmark, we show the agreement between these two simulation protocols in Fig. 2 of the main text.

In both cases, because of the exponential growth 2^τ of the number of leafs in the tree, the simulability of the dynamics is restricted to few iterations. In order to bypass this difficulty, we apply a truncation protocol: after τ^* exact iterations, we only consider the 2^{τ^*-1} highest probabilities to generate the 2^{τ^*} new probabilities for the subsequent time-step. Enforcing normalization $\sum_{j=0}^{2^{\tau^*}-1} p_j^{(\tau)} = 1$, the latter are used to compute the entropy S_t of the trajectory at time $t = \tau\Delta t$. In the low-measurement regime $v < 0$, where all sites are roughly equiprobable, the truncation saturates the entropy growth to a value $\langle S_{\tau > \tau^*} \rangle \sim \ln 2\tau^*$ proportional to the cutoff τ^* . Conversely, in the strong-measurement regime $v > 0$, the few highest probabilities are enough to compute the relevant contribution to the entropy S_t , which we expect to be constant in time: in this case, truncating the full set of p_j 's to the highest 2^{τ^*} values captures the exact dynamics of $\langle S_{\tau > \tau^*} \rangle$, provided τ^* is large enough. In Fig. S1 we show the behavior of $\langle S_t \rangle$ obtained by simulating the protocol as described above, for various values of ϵ .

2. Numerical solution of Eq. (8)

We numerically estimate the behavior of the term $\langle Z \ln Z \rangle_0$ in Eq. (5) of the main text, solving numerically the recursive equation (8) for its generating function. More explicitly, for $K = 2$, we evolve the equation

$$u_{\tau+1}(y) = \left\langle u_\tau \left(y + \ln 2 - \ln \frac{P_1(a)}{P_0(a)} \right) \right\rangle_1 - \frac{1}{2} \left\langle e^{-(y + \ln 2 - \ln P_1(a)/P_0(a))} u_\tau^2 \left(y + \ln 2 - \ln \frac{P_1(a)}{P_0(a)} \right) \right\rangle_1, \quad (\text{SK.1})$$

which is obtained, in the binary tree case $K = 2$, writing $G_\tau(y) = 1 - e^{-y} u_\tau(y)$. Let us note that the above equation reduces to Eq. (SC.1) when neglecting the quadratic term on the r.h.s.. At each time-step τ , we interpolate the function u_τ and evaluate it on the shifted positions $y + \ln 2 - \ln P_1(a)/P_0(a)$, where samples a 's are drawn from a Gaussian probability distribution of mean ϵ and variance 1.

For $\epsilon < \epsilon_c$, corresponding to $v < 0$, the function $u_\tau(y)$ attains a limiting shape, shown in Fig. S2, left panel, corresponding to a finite contribution to the entropy through the integral (9). Conversely, for $\epsilon > \epsilon_c$ and $v > 0$, $u_\tau(y)$ is a wavefront shifting rightwards with velocity v , as displayed in Fig. S2, right panel. Its contribution to the entropy is thus of order $\sim vt$ and cancels out with the one-point terms, yielding $\langle S_t \rangle \sim O(1)$. The latter are displayed on the right panel of Fig. S1, showing complete agreement between the numerical solutions of Eq. (SK.1) and simulations of the dynamics.